5-2020

Magnesium Diboride Embedded Multi-Walled Carbon Nanotube Yarns

Ujjal Lamichhane
The University of Texas Rio Grande Valley

MAGNESIUM DIBORIDE EMBEDDED MULTI-WALLED CARBON NANOTUBE YARNS

A Thesis

by

UJJAL LAMICHHANE

Submitted to the Graduate College of
The University of Texas Rio Grande Valley
In partial fulfillment of the requirements for the degree of

MASTER OF SCIENCE

May 2020

Major Subject: Physics

MAGNESIUM DIBORIDE EMBEDDED MULTI-WALLED CARBON NANOTUBE YARNS

A Thesis
by
UJJAL LAMICHHANE

COMMITTEE MEMBERS

Dr. Karen S. Martirosyan
Chair of Committee

Dr. Mircea Chipara
Committee Member

Dr. Ahmed Touhami
Committee Member

May 2020

ABSTRACT

Lamichhane, Ujjal., Magnesium diboride embedded multi-walled carbon nanotube yarns. Master of Science (MS). May 2020, 55 pp, 3 tables, 25 figures, references 48 titles.

The discovery of superconductivity in a simple hexagonal binary compound of MgB_2 at a relatively high critical temperature ~39 K renewed the interest in the field of superconductivity. Twisted laminar superconducting composite structures based on coiled multi-walled carbon nanotube (MWCNT) yarns were crafted by integrating magnesium and boron homogeneous mixture into the carbon nanotube sheets. After the ignition of the Mg/B/MWCNT system, under the controlled argon environment and uniform heating rate, the high exothermic reaction between magnesium (Mg) and boron (B) with stoichiometric ratio produced the MgB_2/MWCNT superconducting composite yarns. The XRD analysis confirmed that the heated sample consists of a superconducting phase of MgB_2. The tensile strength and Young's modulus of the composite yarn at room temperature have been evaluated to be 200 MPa and 1.27 GPa respectively. The superconductive critical temperature of ~39 K was determined by measuring temperature-dependent magnetization curves. The critical current density was obtained at different temperatures by using hysteresis measurement. The highest value of $J_c = 3.52 \times 10^7$ A/cm^2 was recorded at 5 K.

DEDICATION

To all the victims of COVID- 19 around the globe.

ACKNOWLEDGEMENTS

My first obligation goes to my advisor Dr Karen S. Martirosyan for his continuous support and guidance throughout my education and research. He has been instrumental in my professional growth from the time I have known him. It is my great pleasure to express my sincere gratitude to Dr Ahmed Touhami and Dr Mircea Chipara for their assistance in my education and taking valuable time from their busy schedule to take part in my thesis defence.

At the same time, I heartily acknowledge to Dr Gamage Chamath Dannangoda for his constructive valuable suggestion, support and constant encouragement in improving this research and academic help during the period of my study. I would also like this time to thank Dr Mkhitar Hobosyan and all my lab members for their consistent support throughout the research; without their help and support, this research would not be in this shape today. I would like to express my gratitude to our collaborator from the University of Texas Dallas for providing the carbon nanoforest. I would like to thank Dr Javier Macossay-Torres and his lab group for mechanical properties measurement. Finally, I am thankful to the Department of Physics and Astronomy of our university, The University of Texas Rio Grande Valley for providing me with this opportunity to study and research.

TABLE OF CONTENTS

Page

LIST OF TABLES

Page

LIST OF FIGURES

Page

CHAPTER I

INTRODUCTION

1.1 Background

Superconductivity is the phenomenon in which an electrical current move through a material without resistance. The zero resistance was first discovered by Kamerlingh Onnes (1911) in a solid mercury wire immersed in liquid helium at 4.2 K [1, 2]. Today, the definition of superconductivity is not confined to zero resistance, but it is defined as the set of physical properties of certain materials whose electrical resistances vanishes and from which magnetic flux fields expelled.

Figure 1.1 shows the resistance vs temperature curve for superconductors and non-superconductors. In the case of superconductors, the resistance drops to zero below a certain temperature, called critical temperature (T_c). So, there is no loss of energy in the form of resistance below the critical temperature. Unlike superconductors, all other conductors possess certain resistance at a given temperature. The superconductivity is a quantum mechanical phenomenon characterized by the Meissner effect that shows unique feature of an expulsion of magnetic fields during the superconducting phase [3] as shown in Figure 1.2. It demonstrates the complete ejection of magnetic field lines from the interior of the superconductor during its transitions into the superconducting state. The Meissner effect indicates that superconductivity cannot be understood simply as the idealization of perfect conductivity in classical physics.

Superconductors can be classified as type I or type II. When cooled below its critical temperature, type I superconductors exhibit zero electrical resistivity that displays complete diamagnetism behavior, meaning magnetic fields cannot penetrate it while it is in the superconducting state. A type I superconductor is usually fabricated by using a pure metal while type II superconductors are usually alloys, and transition from a normal state to a superconducting state occurs slowly by passing through an intermediate state. The advantage of a type II superconductor is that the critical field is high enough to allow practical applications.

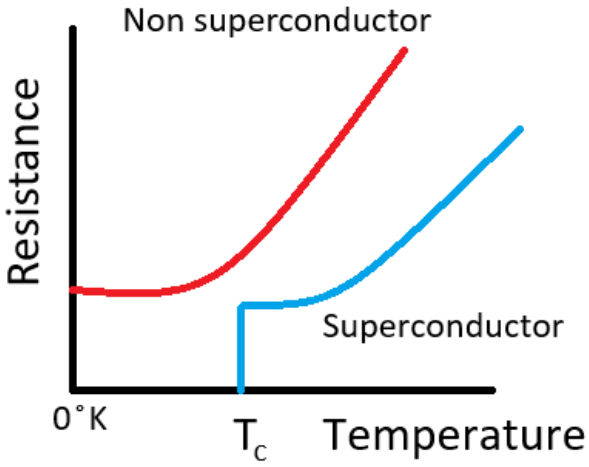

Figure 1.1: The temperature dependence of electrical resistance for superconductor and non-superconductor materials.

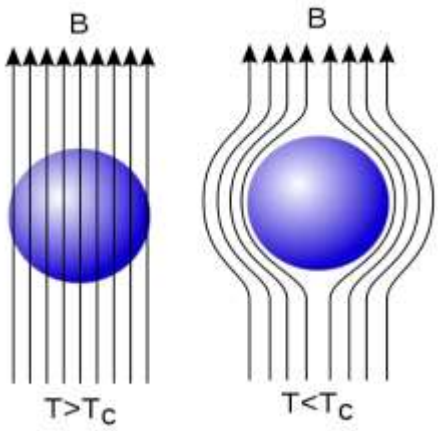

Figure 1.2: Expulsion of the magnetic field above and below the critical temperature.

Most of the physical properties of superconductors vary from material to material. A superconductor is generally considered high-temperature if it reaches a superconducting state above a temperature of 30 K [4]. The applications of superconductors have expanded from electric power transmission and power storage devices to magnetic resonance imaging (MRI) and magnetoencephalography (MEG) [5]. The development of a magnetic levitation train (maglev train) is a practical example of the use of superconducting magnets. The other areas of the application of superconductors include mass spectrometers, particle accelerators, plasma confining in tokamaks, magnetometers and many more.

This thesis is focused on the development of superconducting wires where magnesium diboride (MgB_2) acts as the superconducting active material embedded inside multi-walled carbon nanotube wires. Magnesium diboride can be prepared from the elements magnesium and boron, both of which are easily available in the market for less price. So, the choice of MgB_2 is made for the production of low-cost, high-performance commercial superconducting wire.

1.2 Magnesium diboride

Magnesium diboride (MgB_2) is an inorganic compound with a molar mass of 45.93 g/mol and a density of 2.57 g/cm^3. The melting point of MgB_2 is 830˚C. It was first synthesized by Morton E. Jones and Richard E. Marsh in 1953 [6]. Magnesium diboride can be synthesized by heating the elemental form of magnesium and boron, in the stoichiometric ratio of 1:2, at about 650 ˚C [7]. It is a water-insoluble solid particle with a hexagonal structure. The lattice constants of the hexagonal unit cell are a_0 = 3.0834 and c_0 = 3.5213 Å. The boron plane has strong in-plane SP2 hybridized σ- bonding and more isotropic π bonding connects the plane. In MgB_2, hexagonal honeycomb layers of boron atoms alternate with layers of magnesium atoms, centered on the hexagons. The lattice structure shows the lattice parameter c_0 is greater than the lattice parameter

a_0 which is similar but not much larger like that of high-temperature superconductors (HTS). So, many properties are anisotropic, i.e, it shows different physical properties if measured from a different direction, but not as strongly as in HTS. The unusual bonding arrangement of MgB_2 results in two distinct superconducting bands that in the ideal case have lattice connection as discussed in section 1.3. The chemical equation for the preparation of magnesium diboride can be written as:

$$Mg + 2B \longrightarrow MgB_2$$

Figure 1.3 shows the typical hexagonal (hP3) crystal structure of MgB_2. In the figure, blue-colored boron is enclosed inside the hexagonal structure of light-colored Mg atoms.

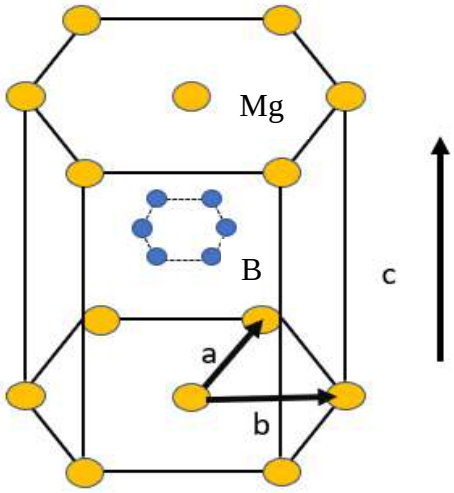

Figure 1.3: Schematic diagram of the MgB_2 crystal structure.

1.3 Magnesium diboride as a superconductor

Even though MgB_2 has been discovered in the early 1950s, its superconducting property was first discovered by Jun Nagamatsu *et al* in 2001 [8]. The critical temperature of MgB_2 is around 39 K, which is considered to be remarkably higher for the binary compound. The relevant mechanism for the superconductivity in this compound is electron-phonon interaction [9]. It is the first compound in which two-gap superconductivity is observed experimentally for

the first time [10]. The two gaps of superconductivity appear due to the presence of two types of electrons at the Fermi level. The electron in the σ-band, being strongly coupled to a phonon, shows strongly superconducting than the electron in π-band having weak electron-phonon coupling. For this reason, MgB_2 is categorized under the type II superconductor. In case of type II superconductor, addition of small amount of impurities can be useful to improve the critical current density of the compound. Alloying the compound can strain the lattice, altering the band structure. In the case of MgB_2, adding carbon causes a contraction of a-axis lattice parameter without any significant changes to the bulk c-axis parameter. For this reason, the addition of carbon sources to MgB_2 can increase the critical current density of MgB_2 which is helpful for the magnetic applications of superconductors.

1.4 Addition of multi-walled carbon nanotubes yarn

Various researches have shown the addition of carbon precursors to MgB_2 increases the critical current density and grain connectivity. Doping carbon nanotubes to the bulk MgB_2 has been researched during the past. However, developing the superconducting yarn by using carbon nanotube could be a novel idea that could not merely increase the critical current density but also increase the current path and the grain connectivity which is an essential part of current transmission. In addition, MWCNT has the outstanding physical and mechanical properties with remarkable strength and a high stiffness up to 300 MPa for single-ply yarns [11], as well as extraordinary electrical, optical and thermal properties [12, 13]. It can carry current densities up to 10^9-10^{11} A/cm^2 [14] and have a thermal conductivity of 3000 W.m/K [15]. Further, the interior thermal stability, heat dissipation and mechanical strength of MgB_2 superconducting wire can be improved by the effect of CNT.

Since MWCNT is very stable even at the high temperature and its melting point is above 3000 ˚C, we can use it to prepare the wire where the MgB_2 layer remains inside the wire. MWCNT sheets extracted from carbon nanoforest, prepared by carbon vapor deposition process [16 - 19], can be scrolled into yarns after loading MgB_2 uniformly on it. MgB_2 can be prepared in situ inside the MWCNT yarn which also helps to prevent the superconducting material reacting with any other oxidizing materials. It is therefore, this research work is mainly concentrated on developing the MgB_2 superconducting wire embedded inside MWCNT yarns.

1.5 Critical current density

The critical current density (J_c) is an important parameter of superconductor. It is the amount of net charges that cross a unit area perpendicular to the flow per second. Higher current density in a superconducting material is an essential aspect of energy transmission, and it is vital to improving it for saving energy and future applications. In the case of pristine MgB_2, J_c decreases rapidly with the increase of the magnetic field due to poor pinning force in the field. The act of magnetic penetration makes the flux pinning possible. It is the phenomenon where a superconductor is pinned above a magnet. So, the introduction of flux pinning is a must to enhance the J_c. The various groups of researchers work in the enhancement of J_c by the introduction of flux pinning. With its large coherence length and two gap superconductivity, many practices including doping with a variety of additives, by using thermo-mechanical processing and magnetic shielding [20, 21] have been introduced in the last decades. The improvement in J_c can be made by the partial substitution of a small amount of dopant which can increase the scattering impurity due to the chemical disorder. The introduction of more pinning centers especially nano-sized second phase inclusions which provide a strong pinning force is essential. The increase of pinning centers served by grain boundaries can significantly increase the J_c value. Among the various dopants, the dopant

of C precursors, including CNT, makes more effective sources compared to other sources because of their high aspect ratio and nanometer diameter [22 - 25]. Also, it can improve the current path and connectivity between the grains in MgB_2.

In this study, MgB_2 superconducting wire is prepared embedded inside MWCNT yarn. In the literature, the increase in the J_c of MgB_2 by the addition of MWCNT can be easily found but nothing about the use of MWCNT as the superconducting wires. Since MWCNT is very stable even at the high temperature, it is possible to perform the combustion reaction inside it. The elemental form of Mg and B powders heated inside the MWCNT wires have large number of pinning centers in the MgB_2 matrix which further helps in the improvement of J_c. MWCNT also serves as a strong conductive framework and provides carbon doping by creating scattering centers to improve the superconducting properties of the wire. In this research, the J_c of the MgB_2 wires is calculated using the beans model and found that the J_c of MgB_2 MWCNT wire has been improved to the order of 10^7 A/cm^2, which is higher compared to the value reported by Kim *et al.*, Shekhar *et al.* [26], M Sawada *et al* [27] and Tolendiuly, S *et al* [28].

1.6 Tensile strength and young's modulus

The tensile strength of a material is the maximum amount of tensile stress that the material can hold before it breaks. It is the measurement of the force required to pull an object up to the breaking point. The value of tensile strength of MgB_2 is low. However, it has larger value in case of MWCNT. The addition of MWCNT in MgB_2 to form MgB_2/MWCNT composite yarn improves the tensile strength of the wire. Increasing the mechanical strength can be useful for the commercial production of superconducting wires.

Young's modulus is another important mechanical property that measures the stiffness of the wire. It is the slope of the tensile stress vs tensile strain curve in the elastic

deformation region of the material. Mathematically, young's modulus can be expressed as the ratio of tensile stress to tensile strain. [29]

$$Young's\ Modulus\ (E) = \frac{Tensile\ Stress}{Tensile\ Strain}$$

Young's modulus has a direct relation with the stiffness. The wire with a higher value of young's modulus is stiffer, i.e. more resistant to bending of the material. It is, therefore, for the commercial production of the wire, the value of young's modulus is expected to be higher. In the case of MgB_2/MWCNT yarn, the value of young's modulus is significantly higher. In this research, the tensile stress at maximum load and young's modulus is calculated and the calculated value is compared with the reported value by G Nishijima, *et al* [30] and Katagiri K, *et al* [31]. The comparison shows the tensile strength of MgB_2/MWCNT composite wire is greater than the MgB_2 wire prepared by the PIT method using Fe-Sheath PIT wire and Cu-Sheath PIT wire.

1.7 Background and current trends

This section is the review of the past works that many groups of researchers had studied in the related topics. Since, after the discovery of MgB_2 as a superconductor, a large group of scientists and researchers are working in this field. Here, the works of some of the teams who were particularly working in enhancing the critical current density of MgB_2 have been studied. Some researches on carbon nanotube doping have been selected for the review purpose. Also, the research work on the effect of heating rates for the preparation of magnesium diboride is presented. The review of past works is helpful to get the proper guidelines for the research. Some reviews of the researches done and published in the past are summarized below.

S.K Chen in his research paper entitled, 'Effect of heating rates on superconducting properties of pure MgB_2, carbon nanotube and nano SiC-doped *in situ* MgB_2 wires' [32] investigated the influence of heating rates and annealing temperatures on the transition

temperatures (T_c) and critical current density (J_c) of pure MgB_2, and carbon nanotube doped in situ monofilamentary MgB_2/Fe wires. The researcher found that for pure MgB_2, J_c was higher with slower heating rates, however, J_c remained to be insensitive to heating rates for the sample doped with carbon nanotubes. Their group had chosen the two isothermal temperatures, 650 ˚C (melting point of Mg) and 850 ˚C which is significantly higher so that the kinetics of phase formation plays an important role in affecting J_c. The team had studied the effect of heating rates by heating the samples at the rates of 100 ˚C/hr and 900 ˚C/hr followed by isothermals at 650 ˚C or 850 ˚C for 30 minutes and then cooling in the furnace to room temperature. He found that for pure MgB_2 sample, T_c was higher for the wire treated at 850 ˚C than 650 ˚C but for CNT doped wire, it was lower than expected for 850 ˚C with slow heating (100 ˚C/hr). Since T_c was depressed in proportion to how much carbon was substituted in the given sample, it suggests that slow heating enhances the substitution of boron for carbon.

In the case of J_c, he observed that CNT doped samples were insensitive to the heating rates. The samples that were heated at 850 ˚C had similar and higher J_c than the sample heated at 650 ˚C regardless of heating rates. It showed a high annealing temperature promotes the C substitution for B, thus enhancing flux pinning in MgB_2. He concluded that the occupation of an intragranular site by an intact CNT was responsible for effective pinning.

However, for pure MgB_2, J_c was higher for slower heating rates. It was because slower heating rate gave the samples more time below the melting point of Mg allowing more MgB_2 to form through solid-state diffusion minimizing the amount of free Mg to attain 650 ˚C. For faster heating rates to high temperatures, more amount of Mg evaporates causing Mg deficiency in the sample.

The research paper entitled 'Alignment of Carbon nanotubes additives for enhancing the magnesium, diboride superconductors' performance' [33] by Shi Xeu Dou *et al* discuss the doping effect of CNT on MgB_2. He concluded that the aligned CNT doped MgB_2 wire showed an enhancement of magnetic J_c by more than an order of magnitude in the high field region. The aligned CNT induced anisotropy in magnetic J_c in relation to the direction of the applied field and significantly improved heat transfer and dissipation during material processing. He believed the electrical and thermal conductivity of CNT doping aided the unusual axial strength to enhance the mechanical properties such as tensile strength and flexibility.

The researcher team also compared the magnetic J_c values for the CNT-doped MgB_2 with undoped MgB_2 as a function of applied field at 5 K and 20 K temperatures. The team observed that for CNT doped MgB_2, the magnetic $J_c(H)$ showed two distinguishing features, (i) a strong anisotropy in relation to the measuring field direction and (ii) a clear enhancement of flux pinning in high field region compared to that of the undoped sample. He also observed the enhancement in $J_c(H)$ performance due to CNT doping was more significant at low temperatures and higher fields.

J.H Kim *et al* in his research paper entitled 'Superconductivity of MgB_2 with embedded multiwall carbon nanotube' [22] observed the critical current density of MWCNT doped MgB_2 wire fabricated by the powder – in – tube (PIT) method and sintered at 900 ˚C temperature. The researcher found MWCNT doped samples sintered at 900 ˚C exhibited $J_c \sim 10^4$ A/cm^2 up to 9 T at 4.2 K which can be explained by lattice distortion and poor crystallinity due to carbon substitution from the MWCNT. In his research, he used MWCNT as the only doping element to MgB_2 but not as a wire. He also observed the critical temperature value for the MWCNT doped sample is lowered than that of the undoped sample. He considered the decrease in T_c was originated from

the effect of band filling of the σ band by electron doping. The researcher further observed the improvement in the J_c performance of MgB_2 samples by doping MWCNT. At 12 T, J_c for MWCNT doped MgB_2 wire had higher order magnitude than the undoped one. He claimed this was due to partial substitution `of C on B sites at the sintering temperature of 900 ˚C which was believed to increase the intra-band scattering and shortening of both mean free path and coherence length.

Chandra Shekhar *et al* in his research paper entitled 'Improved Critical Current Density of MgB_2-Carbon nanotubes (CNTs) composites' [26] claimed the optimum result on J_c was obtained for 10 at. % CNTs admixed MgB_2 sample at 5 K temperature with $J_c \sim 5.2 \times 10^6$ A/cm^2 in the self-field. He observed in MgB_2-10 at. % CNTs sample, there was a comparatively uniform distribution of CNTs within the grains in the MgB_2 matrix which provides flux pinning centers leading to enhancement of J_c. He also studied with different percentages of CNT doping. For MgB_2-25 at. % CNT sample, he observed the dominance of CNTs which masked the flux pinning effect and hence the enhancement in J_c was not as expected to be as high as that for the sample with 10 at. % CNT. He concluded the enhancement of critical current density in the MgB_2-CNTs sample may be attributed to the flux pinning capability of CNTs in the MgB_2 matrix and better grain connectivity. Microstructural features affect crucially the critical current density of superconducting material.

S. Tolendiuly *et al* studied the effect of MWCNT doping on MgB_2 superconducting wire in their research paper, entitled "The effect of MWCNT addition on superconducting properties of MgB_2 fabricated by high-pressure combustion synthesis" [34]. In their research, they prepared the superconducting powder of magnesium diboride doped with MWCNT by the method of combustion synthesis under the argon environment. They observed a sharp superconducting transition temperature at around 38.5 K. they used Beans model to calculate the critical current density and found that high value of critical current density of 1.4×10^8 A/cm^2 at 5 K in zero

magnetic fields for MgB_2 doped with 1% MWCNT. The average grain size of MgB_2 was 3×10^{-5} cm.

1.8 Aims and Objectives

1.8.1 Objectives

The main objective of this study is to develop the superconducting MgB_2/MWCNT composite wire having high critical current density and high tensile strength. The research is carried out to accomplish the following goals:

1. To initiate the ignition of a combustion reaction between magnesium and boron inside the multi-walled carbon nanotube wires.
2. To develop twisted laminar superconducting MgB_2/MWCNT composite yarns.
3. To determine the superconducting properties of MgB_2 /MWCNT wires and compare it with the superconducting properties of MgB_2 powder alone.
4. To improvise the critical current density of MgB_2 superconducting wire by the use of MWCNT.
5. To test the strength of MgB_2/MWCNT wire and compare it with MgB_2 wires.
6. To prepare the superconducting wire of high critical current density.

1.8.2 Significance

The research is mainly related to the enhancement of the critical current density and tensile strength of MgB_2 superconducting wire. Increasing the current density of superconducting wire expands the areas of the use of superconductors for many practical applications such as the transmission of energy and in building Josephson junctions for SQUIDS. Hence, the significance of this research can be summarizing as follows:

1. The research suggests MWCNT is strong enough for the development of commercial superconducting wire.

2. MWCNT helps to increase the current density of MgB_2 superconductor.

3. MgB_2 embedded MWCNT wires can be used for the commercial production of superconducting wire for industrial purposes.

1.8.3 Limitation

Despite the effort of the researcher to make the research errorless, there are some limitations to this research that should be considered as a future work for improvement. The limitations can be listed below:

1. The research was confined to only the small length of the wire (7 cm).

2. Some amount of magnesium escaped out of the wire due to evaporation.

3. The trace amount of magnesium reacts to form MgO on the upper layer of the wire.

4. Difficulty in making the cross-sectional diameter of the wire uniform everywhere.

5. The distribution of MgB_2 powder along the wire cannot be spread-out uniformly.

1.9 Thesis layout

This thesis consists of four chapters. The first chapter 'Introduction' discusses the background and overview of the research. It also provides the summary of the relevant literature regarding the use of ball milling and its timing for the preparation of a homogenous mixture of Mg and B, the effect of temperature and sintering for the reaction of MgB_2 as well as various works done for the improvement of the critical current density of MgB_2 by different attempts.

The second chapter illustrates the experimental procedure used in obtaining the MgB_2 embedded MWCNT wire. It also discusses the various instruments and the applications used for the development of superconducting wire in our research.

The third chapter, 'Results and Discussions', demonstrates all the experimental works and the results along with the discussion about the result obtained. It also provides a comparative study of how the different heating rates of the yarn affect the critical current density and the strength of

the MWCNT yarn. Similarly, the calculation of crystallite size and the comparison of the critical current density of pure MgB_2 and MgB_2/MWCNT composite wire has been discussed in this chapter.

The final chapter is about the conclusion. It concludes our research work as well as discuss the future works that can be done from our research. This chapter also provides the significance of our research work in the area of science and technology especially in the field of nanotechnology and superconductors.

CHAPTER II

METHODS AND MATERIALS

The experiment described later in this thesis all involved the synthesis and analysis of MgB_2/MWCNT yarn composites. The clear understanding of the results of this thesis requires all the ideas of the development of the MgB_2 embedded MWCNT yarn. The purpose of this chapter is to provide background information regarding the scientific instruments used during the synthesis of MgB_2/MWCNT yarn and the process involved in it.

The starting materials used for the experiment include the elemental powder form of magnesium (Mg) and boron (B) and the carbon nanoforest, grown by a chemical vapor deposition process. The scientific instruments used for the synthesis of MgB_2/MWCNT yarn include the rotatory ball miller and differential scanning calorimetry (DSC) whereas the samples were analyzed using scanning electron microscopy (SEM), X-ray diffractometer (XRD), universal testing machine (UTM) and physical property measurement system (PPMS). The brief description of the materials and the scientific instruments used for this research are described in this chapter.

2.1 Magnesium and Boron powder mixture

The superconducting properties of MgB_2 are determined by the quality of the starting Mg and B powders such as purity and particle size of the powders [35]. The most desirable powders would be cheaply available in the market with pure phase and free from contaminants. It has also been reported that the grain connections and J_c values can be enhanced by the Mg and B powders mixture prepared by ball milling [36, 37]. For this research purpose, both magnesium and boron had been purchased from Sigma Aldrich company. The particle size for the Mg used was 20-230

mesh with 98 % purity whereas amorphous B with >95 % pure was used. These powders were mixed in the stoichiometric ratio. For the milling purpose, 30 ml of anhydrous 99.5 % isopropyl alcohol was mixed to 1 gm of the powder mixture. Then the mixture was milled in the rotatory ball miller for 3 hours.

For the milling purpose, 1g of powder mixtures (0.53 g Mg + 0.47 g B) and 30 ml of isopropyl alcohol were kept inside the metallic holder of cylindrical shape having the outer diameter of 5 cm and the inner diameter of 3.8 cm and the length 6.5 cm. 20 small spherical ceramic balls of diameter 1.2 mm and 0.4 g mass were used to mill the mixture. The mixtures were rotated in the Thumler's rotatory ball miller for 3 hours. The purpose of the milling was to mix the Mg and B powders homogeneously in order to receive MgB_2 without any non-reactive initial materials or elements after the combustion reaction. Ultimately, it helps in the grain connectivity after the formation of MgB_2 inside the yarn.

2.2 Multi-walled carbon nanotubes

Multi-walled carbon nanotubes were extracted from carbon nanoforest (Figure 2.1). 30 uniform layers of carbon nanotube sheets were stacked on the top of others which help to increase the strength of the carbon nanotubes. 30 uniform layers of 1.2 cm wide and 7 cm long sheets were stacked to form the layer of multiple sheets of multi-walled carbon nanotubes where the homogenous mixture of the powders prepared after milling was uniformly distributed over the sheet. After the deposition of the powders, MWCNT was twisted to form the yarn.

The carbon nanoforest, from which the multi-walled carbon nanotubes were extracted, were grown by chemical vapor deposition (CVD) onto a <100> silicon wafer bearing 50 nm of thermal oxide and 3 nm of the catalytic iron film [35]. An electron-beam evaporator (CHA-50) was used to deposit the catalytic iron film and the forest growth was conducted in a gas mixture

inside the quartz reactor at atmospheric pressure and 710 ˚C – 750 ˚C temperature for 4 – 10 minutes. The gas mixture contained helium with 56 % H_2 and 5 % C_2H_2 and the flow rate of the gas mixture inside the reactor was 3865 cm^2/min. The synthesized forest had a single carbon nanotube with a diameter of ~ 10 nm. The 280 µm tall forest had a volumetric forest density of 63.8 mg/cm^3. From the side of this nanoforest, multi-walled carbon nanotubes sheets were extracted. Figure 2.2 shows the 30 carbon nanotube sheets stacked one over another.

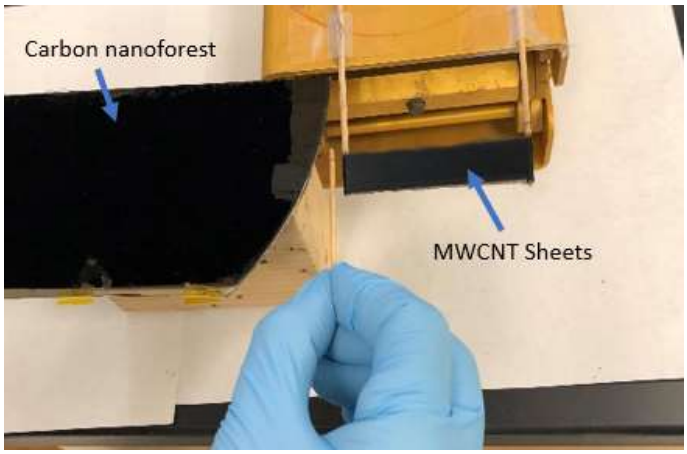

Figure 2.1: Extraction of MWCNT sheets from carbon nanoforest.

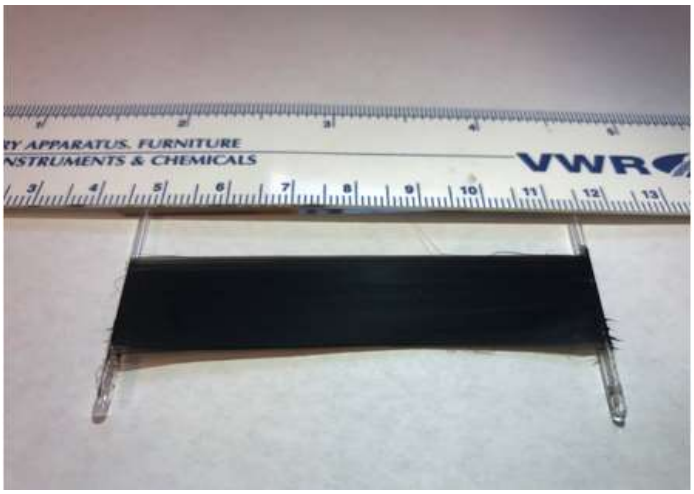

Figure 2.2: Multi-walled carbon nanotubes sheet extracted from carbon nanoforest.

2.3 Differential Scanning Calorimetry (DSC) - Thermo-Gravimetric Analyzer (TGA)

Differential scanning calorimetry was used to heat the twisted yarn. For our experiment purpose, we used the STD-Q600 model DSC-TGA from TA Instrument (Figure 2.3). SDT-Q600 provides the simultaneous measurement of weight change (TGA) and true differential heat flow (DSC) on the same sample from ambient to 1500 ˚C under controlled environment. It is very essential to maintain the proper environment while heating. Many properties of the superconducting yarns like the grain growth, grain connectivity, and the critical current density depend on the heating mechanism of the yarn. In this case, the yarn was heated in a uniform heating rate of 20 ˚C per minute. The heating rate would have an effect on the mechanical properties of the MWCNT yarn as well as on the reaction time. It is important to note that Mg and B powders react to form MgB_2 inside the MWCNT matrix during heating. The melting point of Mg is ~650 ˚C and at this temperature, Mg powder turns into vapor which then reacts with B to form MgB_2. Thus, for a slower heating rate, Mg will vaporize slowly, and the reaction time increases. The MgB_2 thus formed will have better distribution within the yarn and it helps in the grain connectivity, ultimately improving the critical current density of the superconducting yarn. A controlled argon environment was maintained inside the DSC during heating by supplying the ultra-purity argon gas with a flow rate of 100 ml/min. This helps to maintain the inert environment inside the chamber so that Mg would no longer be oxidized by reacting with atmospheric oxygen.

Figure 2.3: STD-Q600 model DSC-TGA from TA instrument.

2.4 Scanning Electron Microscopy (SEM)

The Joel JSM-7100F scanning electron microscope and transmission electron microscope (Figure 2.4) was used for the particle topography and size analysis of our samples. The thermal field emission SEM is an ideal platform for demanding analytical applications as well as those requiring high resolution and ease-of-use. It has a large 5-axis fully eucentric, motorized, automated specimen stage, a one-action specimen exchange airlock, small probe diameter even at large probe current and low voltage, and expandability with ideal geometry for EDS, WDS, EBSP, and CL. The specimen chamber handles specimens up to 200 mm in diameter. Using an electron beam, it also offers all the high-resolution performance of a field emission SEM with the ability to image non-conductive samples within the nano-meters range at moderate to high kV and higher beam current. An electron dispersive x-ray spectroscopy system equipped in SEM helps in the analysis of particle morphology. The clear and high-resolution image from SEM was used to determine the average particle size of the sample with the help of ImageJ software.

Figure 2.4: JSM 7100F scanning electron microscope.

2.5 X-Ray Diffraction (XRD)

In this experiment, X-ray diffraction was used to calculate the phase identification, lattice parameters, and grain size estimation. Bruker D2 Phaser 2nd generation X-Ray diffractometer (Figure 2.5) with Cu-Kα radiation (λ = 1.54056 Å) was used for the measurement. The basic principle for XRD is X-rays is generated by the irradiation of Cu metal with high-energy electrons. The operating parameters for the sources are 40 kV and 30 mA. X-ray photons are emitted as higher energy Cu electrons drop down in energy to fill the vacant orbitals after high energy electrons knock their electrons out of their orbits around the Cu atoms. The emitted x-rays then pass through a monochromator which selects x-rays of the desired wavelength (in our case, Cu-Kα of wavelength 1.54056 Å) to irradiate the sample.

Figure 2.5: Bruker D2 phaser 2nd generation X-Ray diffractometer.

The plane of the crystal lattice of the sample reflects the x-rays irradiated on it. When the x-rays strike on the set of parallel planes of the sample making some angle θ with the normal to the plane, the path length difference of reflected x-rays from each plane would be proportional to Sin(θ). If the path length difference between reflections from the adjacent plane is the integral multiple of wavelength λ, constructive interference occurs which is governed by Bragg's equation [39].

$$n\lambda = 2dSin(\theta)$$

where d is the interplanar spacing. An XRD pattern is generated by plotting diffracted intensity as a function of 2θ. Since 2θ is dependent on d, the XRD pattern can be used to determine the interplanar spacing and lattice parameter. Also, the crystallite size calculation can be carried out by using the Scherrer's relation. Since the XRD pattern is unique for a given sample, it helps to characterize the presence of any substance (MgB_2 in our experiment) in the sample.

2.6 Physical Property Measurement System (PPMS)

Figure 2.6: Physical property measurement system (PPMS) device for magnetic measurement.

The magnetization measurements were performed by using the physical property measurement system (PPMS) having a vibrating sample magnetometer (VSM) attachment. The Quantum Design PPMS Ever Cool II (Figure 2.6) cryogen-free enhancement concept represents the unique in the laboratory equipment with open architecture. The device can be used to measure the heat capacity, AC Susceptibility, normal state resistivity and conductivity, and magnetic moment. For this research purpose, this multifunctional equipment was used for the magnetization measurement with the help of attached the VSM. Zero field-cooling (ZFC) and field-cooling (FC) measurements were performed in the temperature range of 5 K – 50 K with a 100 Oe magnetic field. Hysteresis measurement was performed up to 2 T magnetic field. The shape of the hysteresis curve can be used to confirm the superconductivity state while the width of the hysteresis curve can be utilized to calculate the critical current density of the sample.

2.7 Universal Testing Machine (UTM)

The mechanical properties of the MgB_2/MWCNT wire were studied by measuring the tensile strength and young's modulus of the wire using a universal testing machine (UTM). The UTM also is known as a universal tester, can perform many standard tensile and compression tests on materials, components, and structures. In this research, the tensile strength of MgB_2/MWCNT wire was measured. For the measurement, a cylindrical wire sample of 0.16 mm circular diameter and 3 cm length was taken. The gage length for the measurement was 7.5 mm. The specimen was placed in the machine between the grips and the extensometer. Once the specimen was placed in the machine and the machine started, it began to apply an increasing load on the wire unless the wire deformed. The record of the applied load and the extension of the wire was kept throughout the experiment. The extension of the wire was kept in terms of percentage increase in the length of the wire corresponding to the original length of the wire. The graph between tensile stress vs extension was plotted. The maximum stress applied which broke the wire gives the tensile strength of the wire, whereas the slope of the tensile strength vs extension curve in the elastic deformation region gives the young's modulus of the wire.

2.8 Experimental procedure

Mg and B powder mixture was prepared by mixing Mg (98 %) of 20-230 mesh and B (≥ 95 % amorphous) according to the stoichiometric ratio of 1:2. Isopropyl alcohol (anhydrous, 99.5 %) was introduced to the mixture to prepare for the milling, and the mixture was milled for 3 hours using a rotatory ball miller to receive a homogeneous powder mixture. The mixture was then heated in an oven to evaporate Isopropyl alcohol and prepared for the deposition process.

MWCNT sheets of 1.2 cm wide and 7 cm long were extracted from MWCNT nanoforest grown by chemical vapor deposition (CVD) process. 30 uniform sheets were stacked on top of

each other to increase its strength. The homogenous mixture of Mg and B powders were distributed uniformly on the top of the MWCNT sheets. Then, the twisted laminar yarn was developed by rolling the MgB_2-MWCNT sheets with a low-speed motor under a constant speed of 30 rpm. Then, the yarn was heated at the constant heating rate of 20˚C per minute up to 850 ˚C using differential scanning calorimeter and thermogravimetric analyzer to initiate reaction within the carbon nanotube matrix. Heating was performed under the argon atmosphere with 100 ml/min flow speed.

XRD measurement of the particles was performed to confirm the presence of the MgB_2 phase. The scanning electron microscope equipped with an electron dispersive x-ray spectroscopy system was used for the particle topography and size analysis. The magnetization measurements were performed with the PPMS system having VSM attachment. ZFC and FC magnetization curves were measured in the temperature range 5-50 K using the field of 100 Oe. ZFC measurements were performed by cooling down the sample from 300 K to 5 K without applying any magnetic field. After reaching 5 K, by applying a small magnetic field of 100 Oe, the sample was heated up to 50 K, above the transition temperature, to obtain the ZFC curve. FC curve was obtained by cooling down the sample from 50 K to 5 K while the field is applied. The hysteresis curves were measured up to 2 T at different temperatures of 5 K, 10 K, 15 K, 20 K, and 25 K. For the comparison purpose, MgB_2 was prepared by heating Mg and B powders only and the magnetic measurements were performed in identical ways. The tensile strength of the wire was measured by using the universal testing machine and Young's modulus was determined by calculating the slope of tensile stress vs extension curve in the elastic deformation region.

CHAPTER III

RESULTS AND DISCUSSION

The brief discussion on every result explains the significance of the experiments. The limitations and possible causes are discussed to explain the result clearly. Some experimental procedures are repeated to explain the need for that particular method and the impact of that method in the experiment. In general, this chapter covers all the outcomes of the research work.

3.1 Powder preparation and mixing

One important part of this research is to achieve the higher critical current density of the superconducting yarn. For the higher critical density, it is important that MgB_2 grains should be small (~1 μm). Small grains of MgB_2 not only lead to improve grain connectivity to enhance J_c but also prevent stress concentrations in the matrix which can cause early breakage of the conductor.

In this experiment, the particle size of MgB_2 was not further breakdown after the preparation of the yarn. However, the starting materials, i.e. the elemental form of Mg and B were mixed homogeneously using the rotatory ball milling with the speed of 100 rpm. The ceramic balls used in the milling process helped to well-mix the powder mixture. At the same time, the particle size of the Mg and B also gets reduced. Even though the particle size was not reduced to a bigger extend by the milling, Mg and B powders were mixed homogeneously so that the reaction became uniform during the heat treatment. The milling time of the powder is another important factor to be considered in the reaction. The longer the milling time, the more homogenous is the powder mixture. The milling time of 3 hours was chosen after analyzing the SEM results. It showed the distribution of the Mg and B in the powder mixture was homogenous. The milled powder was

deposited uniformly on the MWCNT sheets. The reaction between Mg and B was performed in-situ inside the MWCNT matrix.

3.2 Combustion reaction

Combustion synthesis is a method used to synthesize materials by exothermic combustion reactions under different environments [40-44]. The process can be carried out through two basic methods, explicitly by front propagation and volume reaction.

Combustion synthesis of MgB_2 integrated in the yarn was done by volume reaction using a DSC-TGA. After the homogenous mixture was made from powder milling and MWCNT sheets were extracted from the carbon nanoforest, MgB_2/MWCNT yarn was prepared by depositing the powder homogenously on the MWCNT sheet and twisting it to form the yarn. Then, the whole yarn was heat-treated in an inert argon environment with a uniform heating rate of 20˚C/min up to 800˚C. Argon environment was chosen to make the inert environment for the heating process. If the environment was not inert, Mg from the sample would have reacted with oxygen to form magnesium oxide (MgO). Thus, an inert environment is preventing Mg from oxidizing.

Figure 3.1 shows the DSC-TGA graph of the mixture of Mg and B powders inside MWCNT. The initial endotherm in the heat flow curve indicates that there is a phase transition (melting) of Mg at around 651 ˚C. Once the Mg melts, it reacts with the B and releases a large amount of heat. This exothermic reaction is visible by the peak around 666.49 ˚C and the amount of heat released was 1033 J/g. During this process, some parts of Mg escaped the system due to vaporization. This is also confirmed by the percentage of the weight change curve. The ~9.14 % decrease in weight percentage after 666 ˚C is due to the loss of some Mg via evaporation.

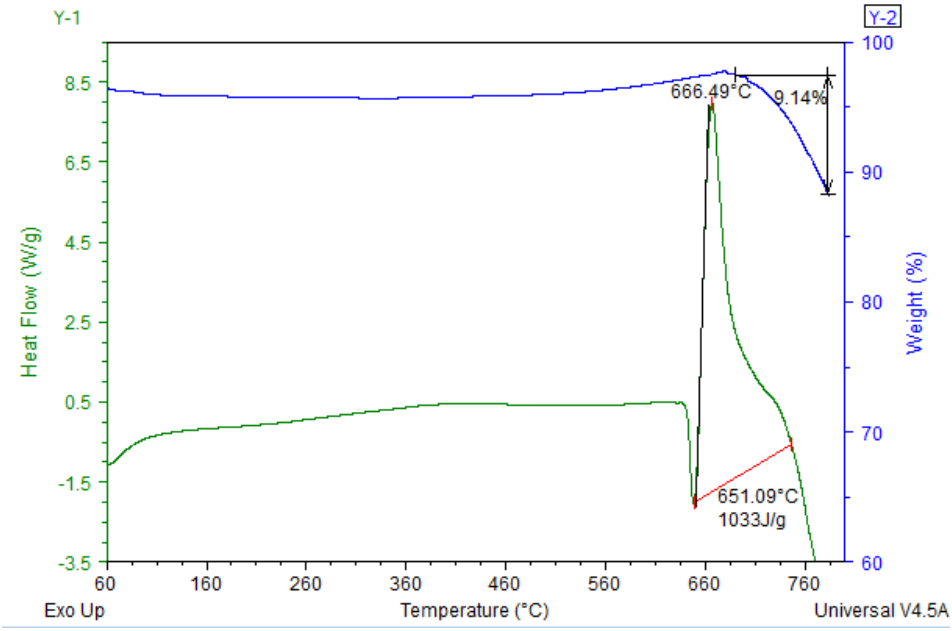

Figure 3.1: DSC plot showing heat flow and change in weight percentage of MgB_2/MWCNT yarn at a heating rate of 20 ºC/min.

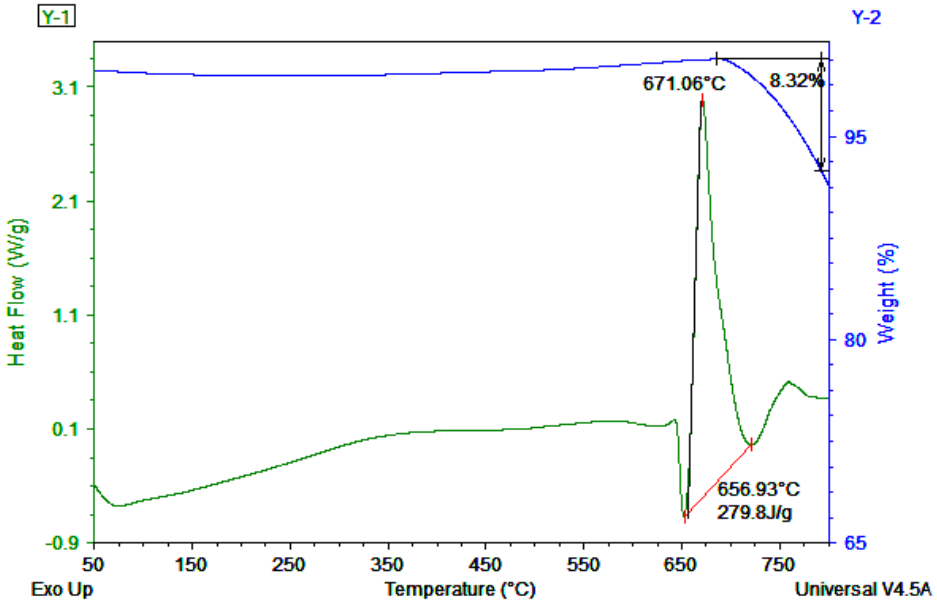

Figure 3.2: DSC plot showing heat flow and change in weight percentage of MgB_2 powder sample at a heating rate of 20 ºC/min.

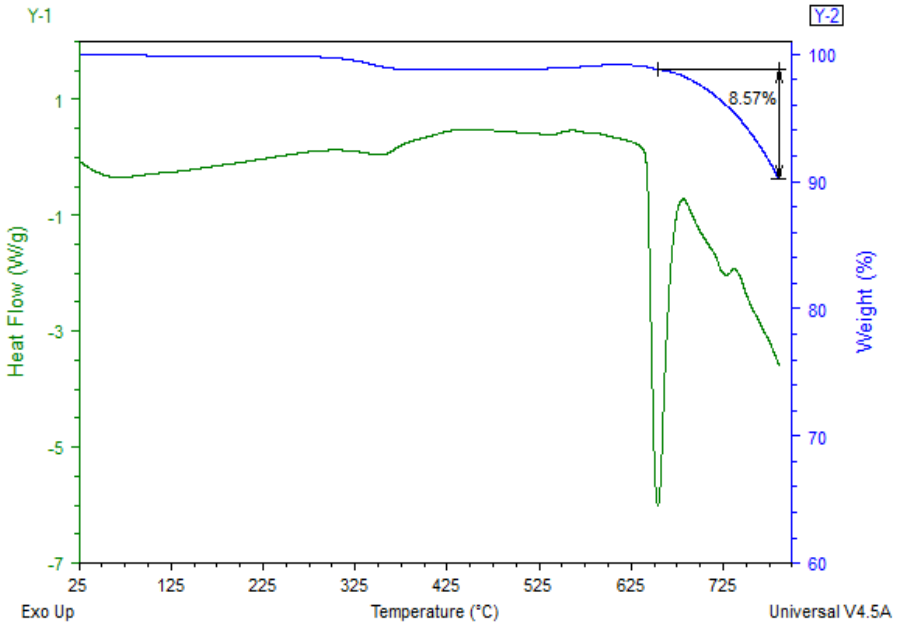

Figure 3.3: DSC plot showing heat flow and change in weight percentage of Mg yarn at a heating rate of 20 ºC/min.

For the comparison, the experiment was conducted with a mixture of Mg and B powders without MWCNT yarn. The experiment was identical but, in this case, the MWCNT was not used and the comparison was done between the MgB_2 and MgB_2/MWCNT yarn composites. Figure.3.2 shows the DSC-TGA result of Mg and B powders under argon environment and uniform heating rate of 20˚C/min up to 800˚C. The comparison of DSC-TGA graph in Figure 3.1 and 3.2 shows that the phase transition temperature (melting) in case of MgB_2/MWCNT yarn was decreased slightly compared to the MgB_2 powder sample. It is because the amount of heat captured inside the yarn creates a slight increase in the pressure inside the yarn and this pressure lowers the melting temperature. However, the difference is not remarkably big enough to create further any effect on the reaction. Similarly, the comparison between the heat release in the exothermic reaction indicates more heat is released in case of MgB_2/MWCNT composite yarn. The greater rate of heat flow indicated the complete reactions occurred inside the yarn. However, the weight loss graph in both cases are comparable. It shows that in both cases, the loss of Mg due to evaporation is similar.

The weight loss in the reaction due to the evaporation of Mg can be confirmed by comparing it with the graph in Figure 3.3. It shows the DSC-TGA results for Mg/MWCNT yarn with an identical experiment. In this case, all the experimental procedure was similar as in the case of Figure 3.1 except the powder inside the yarn was only Mg. If we compare the weight loss graph in Figure 3.1, 3.2 and 3.3, the weight loss is similar in all cases. This proves that the weight loss is due to the evaporation of Mg vapor. To resolve this problem and to maintain the stoichiometric ratio, the amount of Mg was increased by ~10 % while making the powder mixture.

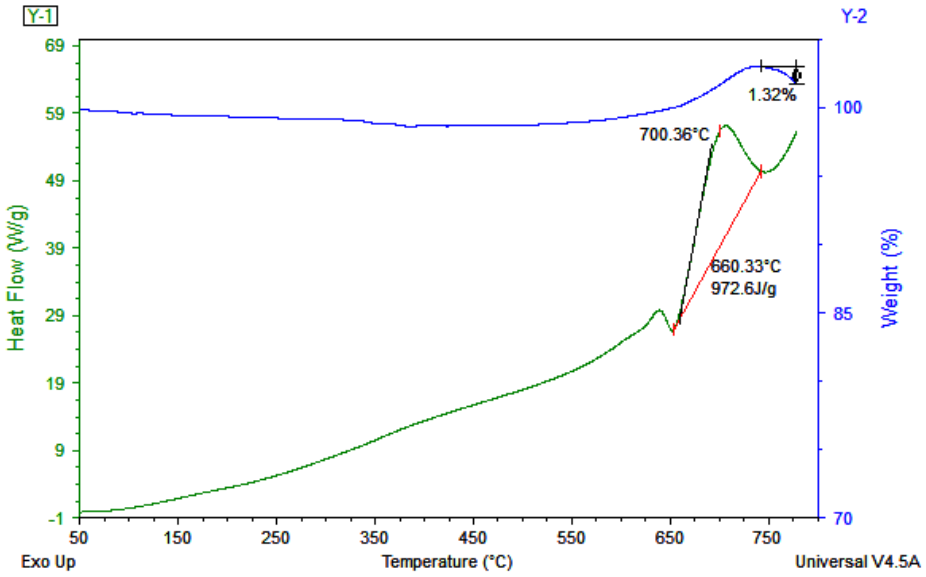

Figure 3.4: DSC plot showing heat flow and change in weight percentage of MgB_2/MWCNT yarn at a heating rate of 50 ºC/min.

For comparison, identical experiments were performed for different heating rates as well. Figure 3.4 shows the DSC-TGA results for MgB_2/MWCNT yarn under the argon environment at a 50˚C/min heating rate. Even though the nature of reactions seemed to be similar in the DSC-TGA plots with different heating rates, the XRD plots showed there remained unreacted boron inside the yarn. Also, the particle size of MgB_2 inside the yarn thus formed was found to be bigger when observed with SEM. This happens because Mg and B got less time for the reaction and all

the reactants do not get enough time to interact. The different experiments proved the best way of heat treatment to the MgB_2/MWCNT yarn is to heat the sample uniformly under the argon environment and the heating rate of 20˚C/min.

3.3 X-Ray diffraction analyses

The final product was characterized by powder X-ray diffraction using Bruker D2 Phaser diffractometer with Cu-Kα radiation (λ =1.5406 Å, 0 < 2θ < 100º) in step size of 0.02º with 0.2s counting time per step. Figure 3.5 shows the XRD plot of the powder mixtures of Mg and B after the milling. To identify the phase of the material, the experimental plots were compared with known database patterns using the QualX software. The graph confirmed the presence of Mg and amorphous B as the starting materials used in the reaction. XRD measurement was performed for the heated yarn and it is given by Figure 3.6. The result confirmed that the reaction was successfully completed by producing a superconducting MgB_2 phase without any trace of the secondary phase in the sample. The experimental peaks exactly matched with the theoretical peak at 2θ = 25.39˚, 33.55˚, 42.49˚, 51.95˚and 59.95˚where θ is the diffraction angle.

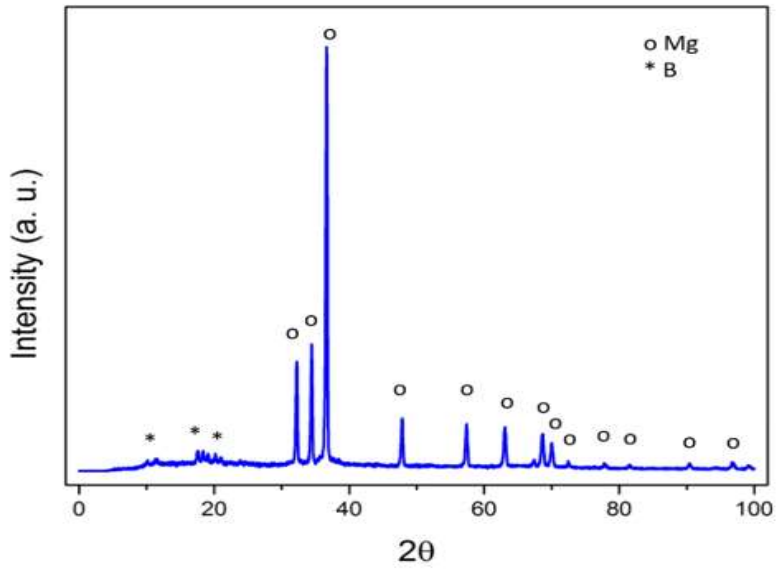

Figure 3.5: XRD plot of Mg and B powders used to make the superconducting yarn.

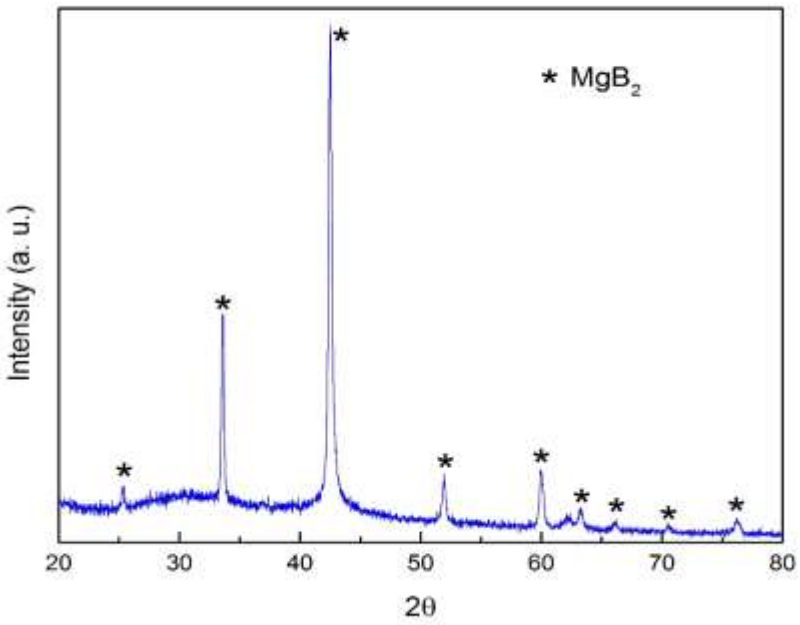

Figure 3.6: XRD pattern of the yarn sample after the heat treatment.

XRD plot was not only used to match with the theoretical plot, but diffraction data also confirmed the hexagonal crystal structure of MgB_2 and the density of 2.628 $g.cm^{-3}$. From the diffraction data, the lattice parameter of the crystal was also found to be a = 3.085 Å and c = 3.523 Å. The diffraction data at various peak values were used to calculate the crystallite size at different peaks.

3.4 Crystallite size calculation

X-ray diffraction measurement not only can be used for qualitative phase analysis but also for quantitative phase analysis such as crystallize size calculation. Crystallite size is the smallest crystal, most likely the single crystal of material in powder form. Particles of any material may present as a single crystal or an agglomeration of several crystals. It means particles cannot be smaller than crystallite size. The crystallite size can be compared with the grain size. The grain morphology is determined by SEM images. If the grain size is larger than the crystallite size, we

can say that the particle is composed up of many crystals agglomerated together. In our case, the particle size obtained from the SEM image was found to be ~ 1 μm whereas the crystallite size, calculated later in this section, was found to be in ~ 40 nm. From this calculation, we can conclude that the MgB_2 grain is agglomerated form of small crystals. This can also be proved from the honeycomb-like hexagonal structures of MgB_2 agglomerated together to form the grain of 1 μm size. The crystallite size calculation was carried out with the help of the Scherrer equation [45]:

$$D = \frac{K\lambda}{\beta Cos\theta}$$

where K is the constant (k = 0.94), λ is the wavelength of X-ray, β is full width at half maximum in radian of the selected peak and θ is the Bragg's diffraction angle.

Table 3.1: Crystallite size calculation for the different peaks of MgB_2

Peak (h k l)	2- Theta	FWHM	Crystallite size (D)
(0 0 1)	25.392	0.243	35.3 nm
(1 0 0)	33.555	0.203	43.1 nm
(1 0 1)	42.488	0.243	36.9 nm
(0 0 2)	51.947	0.223	42.3 nm
(2 1 0)	59.948	0.203	47.7 nm

Table 3.1 shows the crystallite size calculation for different peaks of MgB_2 obtained from the diffraction data of Figure 3.6. For the calculation, the value of full width at half maximum and the Bragg's angle were converted into radian. The calculation shows that the average crystallite size for the MgB_2 particles inside MWCNT yarn is 41.04 nm.

3.5 Particle morphology

The particle size, morphology, and elemental atomic analysis were identified using the thermal field emission scanning electron microscope (SEM, JOEL 7800F) equipped with an electron dispersive X-ray spectroscopy. SEM images were analyzed with the ImageJ software and the average particle size was determined. Since the grain size of the particles of MgB_2 was a few hundred nanometers to few micrometers, the particle morphology, shape and size of the particles can only be analyzed by magnifying to several thousand times. From the analysis of SEM images, a detailed understanding of the particle's overall morphology can be studied. These analyses were useful for the determination of various other properties of the material.

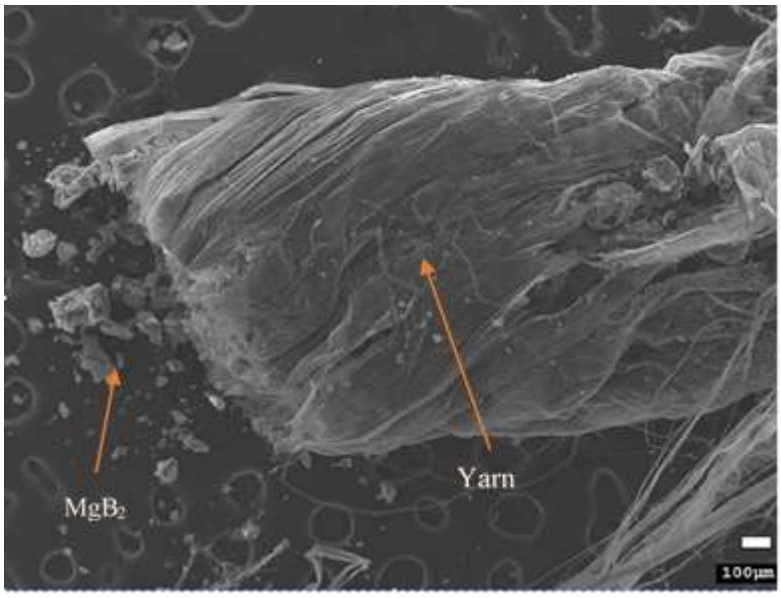

Figure 3.7: SEM image of the MgB_2/MWCNT yarn sample.

Figure 3.7 is the image captured of the MgB_2/MWCNT yarn. One end of the yarn was cut to display the particles were present inside the yarn. The cylindrical-shaped yarn has a width of 0.2 mm inside which the MgB_2 layer remains as shown in figure 3.8.

.

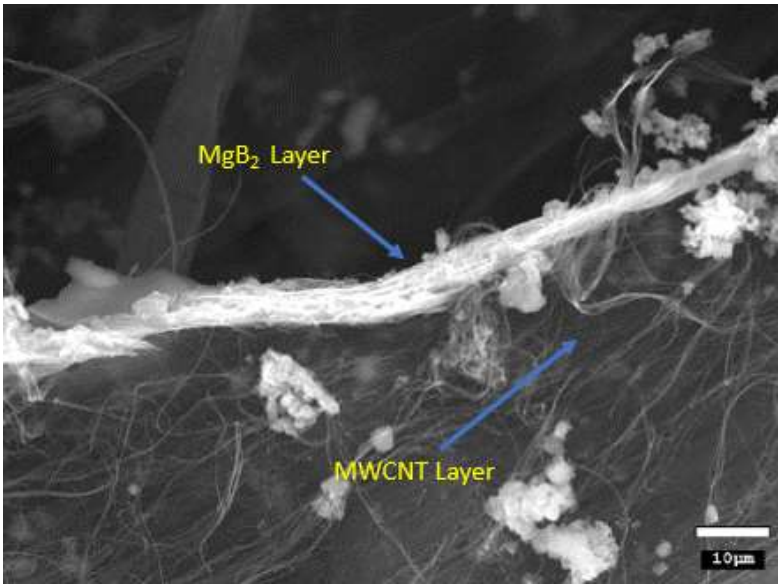

Figure 3.8: MgB_2 powder inside the MWCNT yarn as seen from SEM image.

The shining layer in the middle of Figure 3.8 was MgB_2 and the side tubes were carbon nanotubes. The yarn was cut from the top of the wire and the inside continuous superconductive layer of MgB_2 was visible. This image proved that there was a continuous wire-like structure inside the yarn. So, it can be presumed that current can flow through the sample continuously, thus, the yarn could be used as the superconductive wire.

Figures 3.9 (a) and (b) are the images of MgB_2 grain and crystals captured with SEM. Many MgB_2 crystals agglomerated to form grain was captured in Figure 3.9 (a). The honey comb like layers of hexagonal MgB_2 were arranged together to form the big grain. Figure 3.9 (b) was magnified to see the MgB_2 crystals. These images captured by magnifying up to 25000 times were used to calculate the particle size of MgB_2 grains inside the MWCNT yarns. ImageJ software was used to calculate the average particle sizes in the image. The average particles size was determined to be 1 μm. However, the average particles size for pure MgB_2 was determined as 26 μm. By comparing the values of MgB_2/MWCNT yarn and pure MgB_2 sample, it is apparent that the

particle is lower in MgB_2/MWCNT sample. This smaller size of MgB_2 helped in the increment of the critical current density of the wire as shown in the calculation of magnetic measurement section.

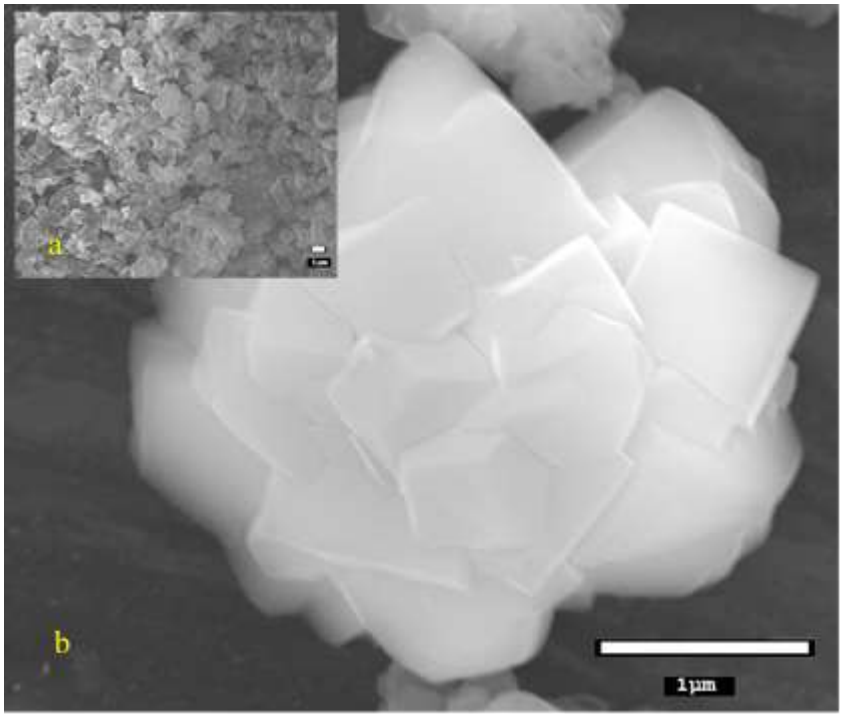

Figure 3.9: (a) SEM image of MgB_2 crystal inside MWCNT yarn and (b) MgB_2 grain inside MWCNT yarn.

3.6 Magnetic measurement

The temperature dependence of the magnetization curve is shown in figure 3.10. zero-field-cooling (ZFC) and field-cooling (FC) magnetization curves were measured in the temperature range 5-50 K using a magnetic field of 100 Oe. ZFC measurements were performed by cooling down the sample from 300 K to 5 K without applying any magnetic field. After reaching 5 K, by applying a small magnetic field of 100 Oe, the sample was heated up to 50 K, above the transition temperature, to obtain the ZFC curve. FC curve was obtained by cooling down the sample from

50 K to 5 K while the field is applied. The curve shows that the superconducting transition temperature for MgB_2 wire is around 37.5 K. If we compare the temperature-dependent magnetization measurement of the MgB_2/MWCNT yarn with the pure MgB_2 powder, i.e. 39 K as shown in Figure 3.11, the superconducting transition temperature for the MgB_2/MWCNT yarn seems to be slightly lowered. But the temperature is still comparable to the theoretical critical temperature for MgB_2. The slight decrease in the critical temperature is due to the CNT doping effect with MgB_2 from the MWCNT yarn. Thus, we can assume that some inner part of the MWCNT yarn also acts as the carbon doping source for MgB_2. This doping effect can also be predicted from the calculation of critical current density. The critical current density of MgB_2/MWCNT yarn has been highly increased compared to the critical current density of MgB_2.

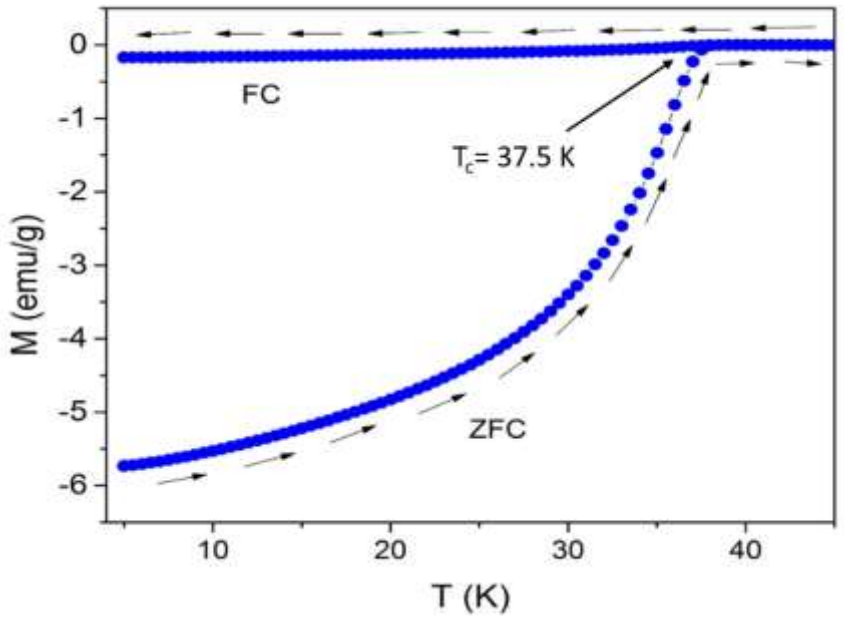

Figure 3.10: Temperature dependence magnetization curve for MgB_2/MWCNT yarn.

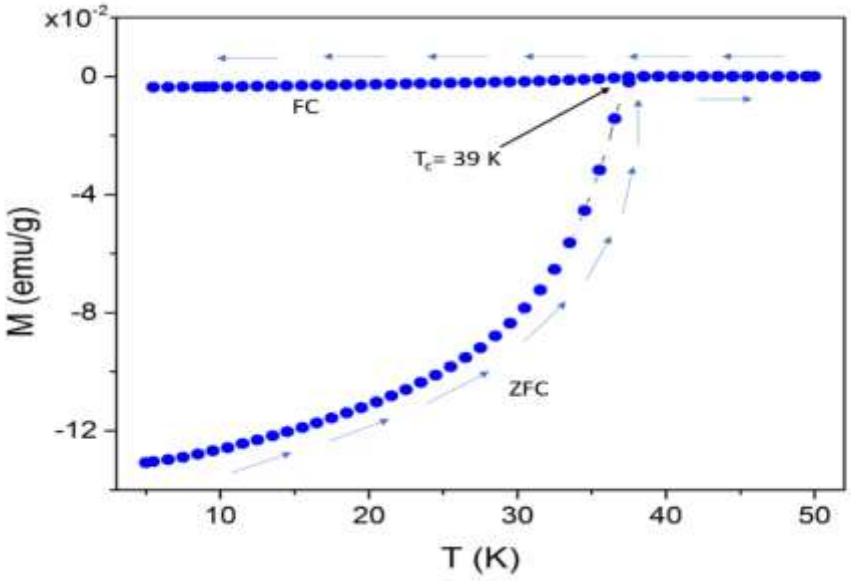

Figure 3.11: Temperature dependence magnetization curve for pure MgB_2 powder sample.

Hysteresis measurement was done to characterize the magnetic behavior of any material. The hysteresis loop of any magnetic material distinguishes the specific magnetic properties of that material. The hysteresis loop shown in figure 3.12 for MgB_2/MWCNT yarn is the characteristic behavior of type II superconductor which confirms that MgB_2/MWCNT yarn is superconducting. The typical type II superconductor is the one which exhibits an intermediate phase of the mixed ordinary and superconducting properties at an intermediate temperature and magnetic field above the superconducting phase. The most important difference between type I and type II superconductors is that the surface energy of the superconducting/normal interface in the case of type II superconductors is negative [46,47].

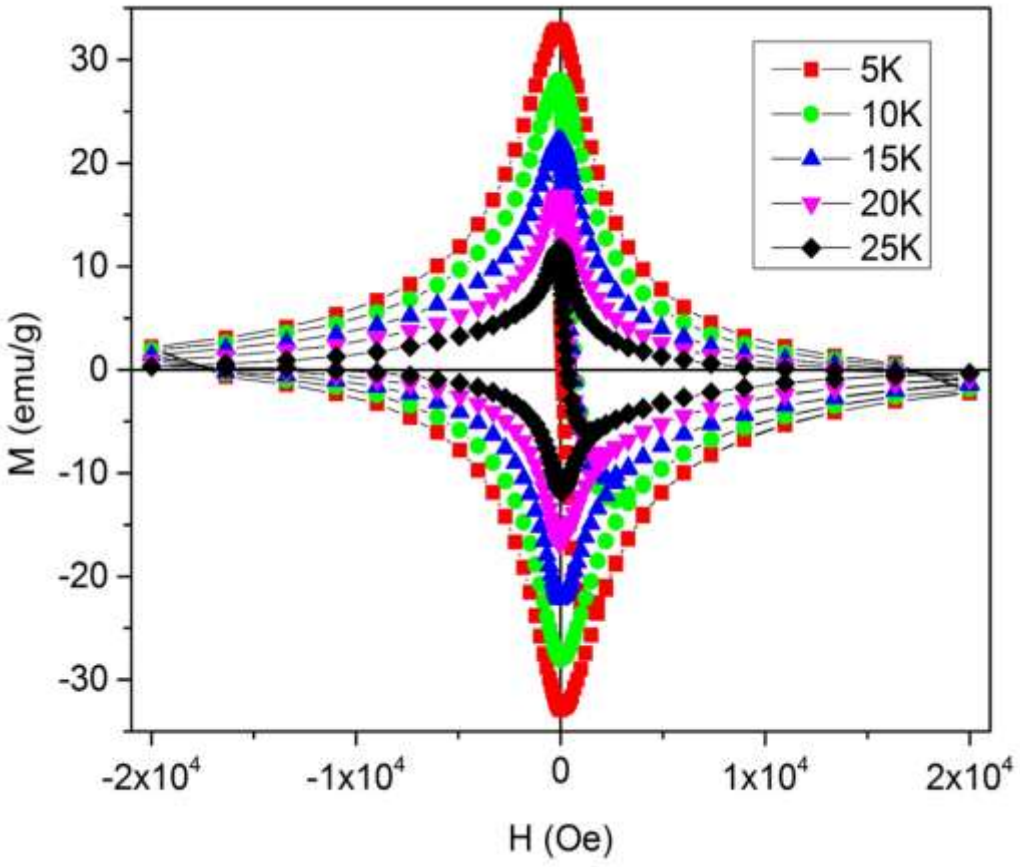

Figure 3.12: Hysteresis curve of MgB_2/MWCNT Yarn up to 20 kOe (2 Tesla) at different temperatures.

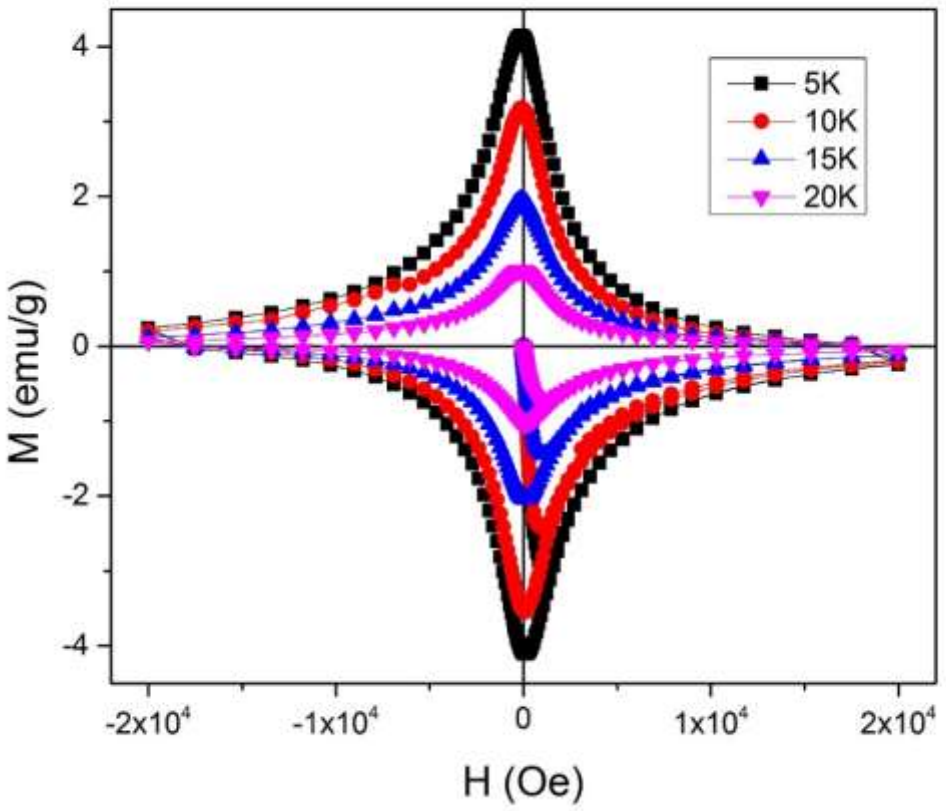

Figure 3.13: Hysteresis curve of MgB_2 powder up to 20 kOe (2 Tesla) at different temperatures.

Figures 3.12 and 3.13 are the hysteresis diagrams of MgB_2/MWCNT yarn and MgB_2 powder respectively. For both cases, the maximum magnetic field of 2 T was applied, and the hysteresis measurement was performed for different temperatures. The width (between highest and lowest M values for a given magnetic field) of the hysteresis curve at the point of the expulsion of the magnetic field was used to calculate the critical current density of the material used. The comparison of Figure 3.12 and 3.13 clearly shows that the width of the hysteresis curve increases nearly 10 times in the case of MgB_2/MWCNT yarn in comparison to MgB_2 powders. Since the critical current density depends on the width of the hysteresis curve and the grain size of the sample, it can be inferred from the above diagram that the critical current density in the case of

MgB_2/MWCNT is much higher than the pure MgB_2. It is apparent from the graphs that as a typical superconductive behavior the width of the hysteresis loop decreases while the temperature increases for both samples. The width, 67 emu/g, recorded for 5 K temperature was the highest obtained and it gradually decreased to the lowest value of 25 emu/g, where the temperature was at 25 K. This also infer the behavior of the critical current density of a superconductor, where J_c increases while the temperature decreases.

3.7 Calculation of critical current density

The critical density for any superconductor is the amount of charge per unit time that flows through the unit cross-section area. The critical current density of the yarn can be calculated by using the Bean's model [48].

$$Jc = 20\frac{\Delta M}{d}$$

$$\Delta M = M^+ + M^-$$

where ΔM is the difference between magnetization M in increasing and decreasing magnetic fields (emu/cm^3), d is the average grain size. It shows the value of J_c depends on the magnetization width of the hysteresis curves and the particle size of the material. Since the width of the hysteresis loop increases as the temperature decreases, the critical current density at 5 K is higher compared to the critical current density at 25 K.

Table 3.2 shows the calculation of J_c values of MgB_2/MWCNT yarn using Bean's formula. The critical current density versus temperature graph in figure 3.14 represents that the critical current density increases with lowering the temperature. For the comparison, the J_c value of pure MgB_2 powder was also calculated and given in table 3.3 and figure 3.15. For both calculations, the hysteresis width for different temperatures was obtained from the hysteresis curves in figures 3.12 and 3.13. The particle sizes were determined using SEM analysis. The particle size of 1 μm for

MgB_2/MWCNT composite yarn and 26 μm for pure MgB_2 was used in the calculation. Similarly, the density, 2.628 g/cm^3, calculated from diffraction data, was used to convert the values to emu/cm^3.

Table 3.2: Calculation of J_c of MgB_2/MWCNT yarn

Temperature (K)	Width of Hysteresis curve (emu/g)	Critical current density (A/cm^2)
5	67	3.52 x 10^7
10	58	3.05 x 10^7
15	46	2.41 x 10^7
20	37	1.94 x 10^7
25	25	1.31 x 10^7

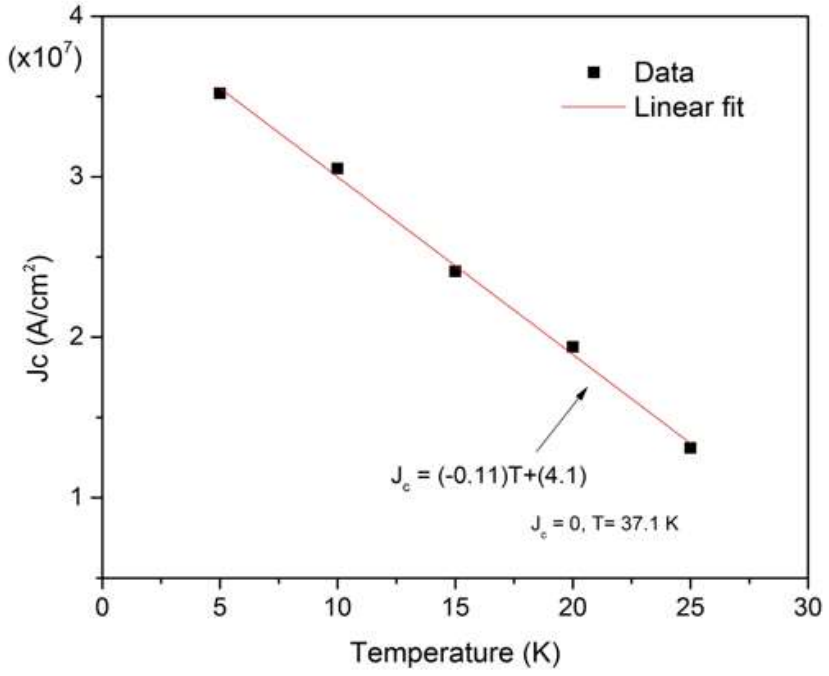

Figure 3.14: Critical current density vs temperature for MgB_2/MWCNT yarn.

Table 3.3: Calculation of J_c of pure MgB_2.

Temperature (K)	Width of Hysteresis curve (emu/g)	Critical current density (A/cm^2)
5	8.2	1.62×10^5
10	6.7	1.32×10^5
15	4.1	7.9×10^4
20	2.0	3.95×10^4

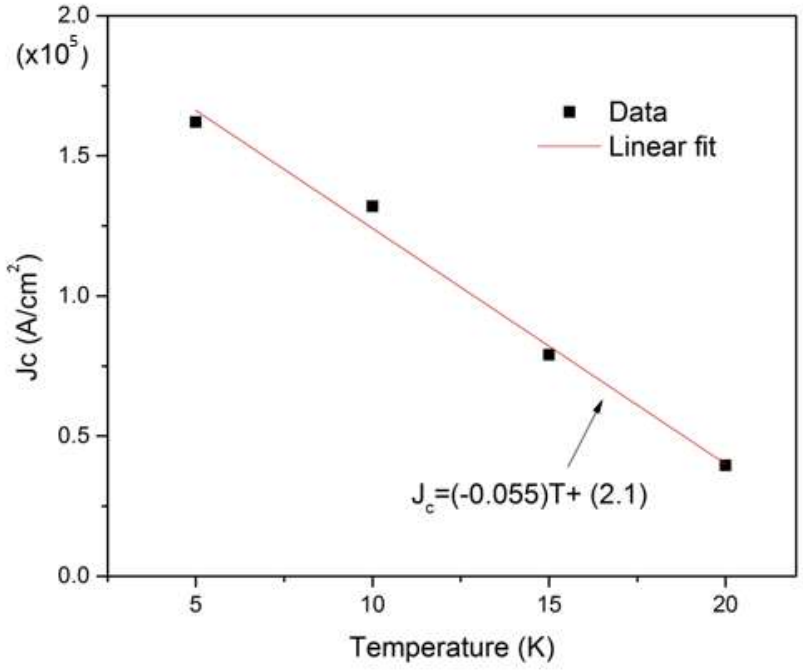

Figure 3.15: Critical current density vs temperature for MgB_2 powder.

When comparing both Jc values from table 3.2 and 3.3, it is noticeable that the J_c values in the case of MgB_2/MWCNT are higher than the J_c values for pure. Also, the highest value of J_c obtained in this experiment was 3.52×10^7 A/cm^2 for MgB_2/MWCNT yarn at 5 K temperature. The comparison of the J_c values for MgB_2/MWCNT yarn and pure MgB_2 powder reveals that the J_c value for MgB_2/MWCNT yarn is around 100 times greater than the pure MgB_2. The greater

hysteresis width and smaller particle size both helped MgB_2/MWCNT to obtain a greater value of the critical current density. Also, if we compare the values of the critical current densities at different temperatures, the J_c values were greater for lower temperatures in both cases. The main reason for the increase in the J_c values for MgB_2/MWCNT composite yarn is due to the increase in the number of pinning centers to the MgB_2 matrix prepared in situ. MWCNTs also serve as a strong conductive framework and provide carbon doping by creating scattering centers to improve the superconducting properties of the yarn.

Figure 3.14 and 3.15 shows the linear relation of critical current density with the change in temperatures. The negative slope indicates the increase in critical current density by lowering the temperature. By extrapolating the fitted curve to ~ 0 K, the maximum (theoretical) value for the critical current density can be obtained. The maximum values of $J_c = 4.1 \times 10^7$ A/cm^2 and 2.1×10^5 A/cm^2 were estimated for the MgB_2/MWCNT and MgB_2, respectively. Similarly, extrapolating the curve to $J_c \sim 0$ A/cm^2 shows the temperature values, which are stated on the graphs, are close to the critical temperature (Tc) of the sample. The obtained values of temperature for $J_c \sim 0$ are similar to the values obtained from ZFC/FC measurement.

Further, the obtained J_c values in this experiment for MgB_2/MWCNT yarn are greater by the order of 10 than the values obtained by M Sawada *et al*, [27] ho used MgB_2C_2 as the carbon source dopant to prepare carbon-doped MgB_2 bulk by in-situ powder in the closed-tube method. Similarly, the reported value of J_c by Sekhar *et al*,[26] who studied the doping/admixing of carbon nanotubes in different concentrations in MgB_2 and the value obtained from Kim *et al* [22] by doping CNTs in MgB_2 prepared from PIT method is also lower than the J_c value calculated in this research. This shows the improved value of J_c for MWCNT yarn over CNT doping to MgB_2.

3.8 Tensile strength measurement

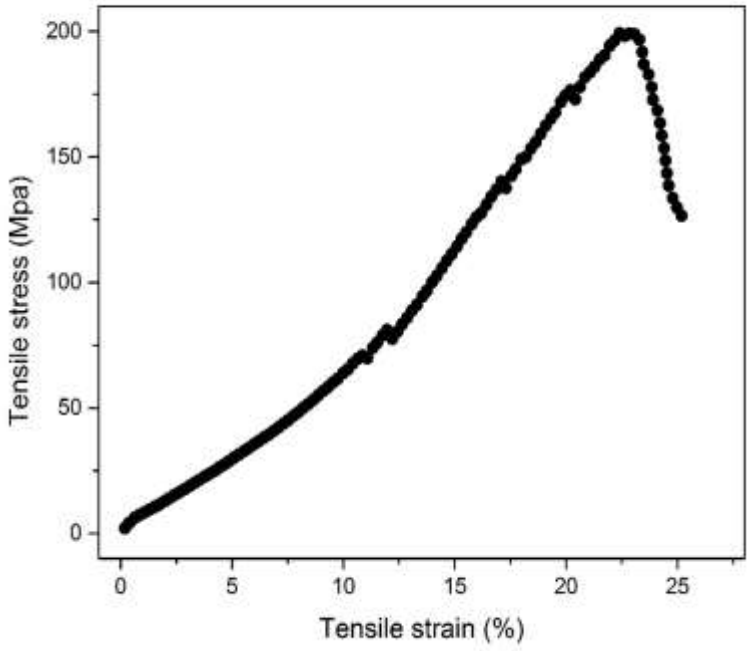

Figure 3.16: Tensile strength measurement of MgB_2/MWCNT yarn.

The tensile strength measurement of the sample is shown in Figure 3.16. The measurement was performed using a universal testing machine. The tensile stress at maximum load was found to be 200 MPa with the extension of 23 % and the young's modulus was calculated to be 1.25 GPa. The obtained tensile strength was compared with the values reported by G Nishijima, *et al* [30] and Katagiri K, *et al* [31]. The transverse compressive stress of the Fe- Sheath PIT processed wire was reported to be 160 MPa and the strain of 0.51 % and the internal Mg diffusion (IMD) process wire to be 206 MPa and 0.67 % respectively by G Nishijima and the research team. The irreversible transverse compressive stress as reported by Katagiri K, and the team for Cu- Sheath PIT processed MgB_2 wire was 150 MPa. The comparison of these values with our result proved that the tensile strength of MgB_2/MWCNT composite yarn is greater than the MgB_2 wire developed by the PIT method and comparable to the wire prepared by the IMD process. Also, the extension of the wire

prepared by both methods, the PIT and IMD process seemed to be greater. The greater values of strain lead to the lower value of young's modulus which implies that the MgB_2/MWCNT composite wire is stiffer to bending. For the commercial production of superconducting wire, the stiff wire with more tensile strength is expected. This proves that MgB_2/MWCNT composite yarn can be a promising candidate for the commercial production of superconducting wire.

CHAPTER IV

CONCLUSIONS AND SUMMARY REMARKS

The research presented in this thesis focused on the development of low-cost, high-performance commercial MgB_2 superconducting wire with high critical current density. The most important part of this research project was the use of MWCNT as a yarn. This innovative idea of developing a superconducting wire by using thermally stable MWCNT as the yarn inside which the elemental form of Mg and B reacted to form a superconducting phase resulted to improve the critical current density of MgB_2 inside the MWCNT matrix to the order of 10^7 A/cm^2.

The mechanical properties of the MWCNT added to the superconducting properties of MgB_2 to produce superconductive wire can be used in the multiple superconductor applications. The major limitations of the MgB_2 superconducting wires produced so far includes the lower value of critical current density and the fallible nature of the MgB_2 wire. MgB_2/MWCNT composite wire can be the best alternatives to overcome these limitations.

A proof of the concept of superconducting wire was presented in this research study. The elemental form of Mg and B powders and carbon nanoforest were used as the starting materials. Ball milling of the powder mixtures were used, and the samples obtained from different trails were compared. The best way to make the homogenous mixture was to mix the sample with a little amount of non-reacting volatile liquid (e.g. isopropanol) and milled in the ball miller for more than 3 hours. A better result was obtained for a longer period of ball milling; however, 3 hours of milling was enough to make a homogenous powder.

The stack of the MWCNT sheets prepared to make the multi-walled nanotubes yarn should be identical and the distribution of the homogenous powder on it should be uniform. The twisted yarn should be prepared in such a way that the width of the yarn would equal through-out the yarn. The proper distribution of the powder mixtures and the well-prepared yarn ensure in the smooth reaction of Mg and B inside the MWCNT matrix during the heat treatment.

The thermal analysis of the DSC-TGA graph confirmed the exothermic reaction took place just above the melting point of magnesium. It inferred the phase change of the reactant and the reaction between Mg and B occurred releasing the huge amount of energy. The change in weight curve reflected the loss of weight of the reactant by about 10 % after the melting point of Mg. The loss of weight was due to the escaping of Mg vapor. Thus, to maintain the stoichiometric ratio, an extra 10 % by weight of Mg was added to the initial powder to minimize the unreacted B inside the yarn. The formation of a continuous MgB_2 superconducting layer inside the yarn was confirmed from the SEM image. XRD graph confirmed the phase of the material inside the yarn as MgB_2. The hysteresis plots from magnetic measurement further clarified that the wire had type II superconductive properties. Also, the critical temperature of the wire was calculated and was obtained slightly less than the critical temperature of pure MgB_2. It was due to the carbon source from the MWCNT. However, the critical temperature was comparable to the theoretical value.

The calculation of critical current density showed an improved value than the pristine MgB2. The carbon source from MWCNT provided more pinning force to increase the value of Jc significantly. It was found that addition of MWCNT increases the J_c by 100 times compared to pure MgB_2. Increasing the value of critical current density is vital for superconducting properties, therefore, it opened the door to many applications of superconducting wires. For the practical superconductor, its Jc value is always expected to be higher.

In addition to the critical current density, the mechanical properties of MWCNT can also be useful to develop the superconductive wire. The increase in the tensile strength and young's modulus of MgB_2/MWCNT wire compared to pure MgB_2 wire opens the possibility of commercial MgB_2/MWCNT wire production. This research concluded that the tensile strength and Young's modulus of MgB_2/MWCNT composite yarn are greater than the MgB_2 wire developed by the PIT method. Thus, MgB_2/MWCNT composite yarn can be a promising candidate for the production of commercial superconducting yarn.

In retrospect, the use of MWCNT as the yarn to make MgB_2/MWCNT composite yarn can be the best way for the production of low-cost, high-performance commercial superconducting wire since the mechanical properties, as well as critical current density of MgB_2 both, improved in case of MgB_2/MWCNT composite superconducting wire.

REFERENCES

1. Blundell, Stephen, Superconductivity, A Very Short Introduction. (Oxford University Press, 1st edition , p. 20, 2009
2. van Delft, D. (2012). History and significance of the discovery of superconductivity by Kamerlingh Onnes in 1911. *Physica C: Superconductivity*, *479*, 30-35.
3. Hirsch, J. E. (2012). "The origin of the Meissner effect in new and old superconductors". Physica Scripta. 85 (3): 035704.
4. Grant, Paul Michael, The great quantum conundrum. Nature. 476 (7358): 37–39, 2011.
5. Wheless, J. W., Castillo, E., Maggio, V., Kim, H. L., Breier, J. I., Simos, P. G., & Papanicolaou, A. C. (2004). Magnetoencephalography (MEG) and magnetic source imaging (MSI). *The neurologist*, *10*(3), 138-153.
6. Jones, M. E., & Marsh, R. E. (1954). The preparation and structure of magnesium boride, MgB2. *Journal of the American Chemical Society*, *76*(5), 1434-1436.
7. Przybylski, K., Stobierski, L., Chmist, J., & Kołodziejczyk, A. (2003). Synthesis and properties of MgB2 obtained by SHS method. *Physica C: Superconductivity*, *387*(1-2), 148-152.
8. Nagamatsu, J., Nakagawa, N., Muranaka, T., Zenitani, Y., & Akimitsu, J. (2001). Superconductivity at 39 K in magnesium diboride. *nature*, *410*(6824), 63.
9. Xue, Y., Asada, S., Hosomichi, A., Naher, S., Xue, J., Kaneko, H., ... & Akimitsu, J. (2005). X-ray Diffraction Study of MgB 2 at Low Temperatures. *Journal of low temperature physics*, *138*(5-6), 1105-1115.

10. Suhl, H., Matthias, B. T., & Walker, L. R. (1959). Bardeen-Cooper-Schrieffer theory of superconductivity in the case of overlapping bands. *Physical Review Letters*, *3*(12), 552.

11. Zhang, M., Atkinson, K. R., & Baughman, R. H. (2004). Multifunctional carbon nanotube yarns by downsizing an ancient technology. *Science*, *306*(5700), 1358-1361.

12. Zakhidov, A. A., Baughman, R. H., Iqbal, Z., Cui, C., Khayrullin, I., Dantas, S. O., ... & Ralchenko, V. G. (1998). Carbon structures with three-dimensional periodicity at optical wavelengths. *Science*, *282*(5390), 897-901.

13. Ulbricht, R., Lee, S. B., Jiang, X., Inoue, K., Zhang, M., Fang, S., ... & Zakhidov, A. A. (2007). Transparent carbon nanotube sheets as 3-D charge collectors in organic solar cells. *Solar Energy Materials and Solar Cells*, *91*(5), 416-419.

14. Wei, B. Q., Vajtai, R., & Ajayan, P. M. (2001). Reliability and current carrying capacity of carbon nanotubes. *Applied Physics Letters*, *79*(8), 1172-1174.

15. Kim, P., Shi, L., Majumdar, A., & McEuen, P. L. (2001). Thermal transport measurements of individual multiwalled nanotubes. *Physical review letters*, *87*(21), 215502.

16. R. H. Baughman, A. A. Zakhidov, and W. A. de Heer, "Carbon nanotubesthe route toward applications," Science 297(5582), 787–792 (2002).

17. M. Zhang, K. R. Atkinson, and R. H. Baughman, "Multifunctional carbon nanotube yarns by downsizing an ancient technology," Science 306(5700), 1358–1361 (2004).

18. A. A. Zakhidov, R. H. Baughman, Z. Iqbal, C. Cui, I. Khayrullin, S. O. Dantas, J. Marti, and V. G. Ralchenko, "Carbon structures with threedimensional periodicity at optical wavelengths," Science 282(5390), 897–901 (1998).

19. R. Ulbricht, S. B. Lee, X. Jiang, K. Inoue, M. Zhang, S. Fang, R. H. Baughman, and A. A. Zakhidov, “Transparent carbon nanotube sheets as 3-D charge collectors in organic solar cells,” Sol. Energy Mater. Sol. Cells, 91(5), 416–419 (2007).

20. Okayasu, S., Sasase, M., Hojou, K., Chimi, Y., Iwase, A., Ikeda, H., ... & Maeda, A. (2002). Irradiation effects on MgB2 bulk samples and formation of columnar defects in high-Tc superconductor. *Physica C: Superconductivity*, *382*(1), 104-107.

21. Serrano, G., Serquis, A., Rodrigues Jr, D., Malachevsky, M. T., Espasandin, J. M., & Ayala, C. (2008). Effects of sheath materials and thermo-mechanical treatments on the superconductivity of MgB2 wires and tapes. In *Journal of Physics: Conference Series* (Vol. 97, No. 1, p. 012127). IOP Publishing.

22. Kim, J. H., Yeoh, W. K., Xu, X., Dou, S. X., Munroe, P., Rindfleisch, M., & Tomsic, M. (2006). Superconductivity of MgB2 with embedded multiwall carbon nanotube. *Physica C: Superconductivity and its applications*, *449*(2), 133-138.

23. Dou, S. X., Yeoh, W. K., Horvat, J., & Ionescu, M. (2003). Effect of carbon nanotube doping on critical current density of MgB 2 superconductor. *Applied physics letters*, *83*(24), 4996-4998.

24. Kim, J. H., Yeoh, W. K., Qin, M. J., Xu, X., & Dou, S. X. (2006). The doping effect of multiwall carbon nanotube on Mg B 2/ Fe superconductor wire. *Journal of applied physics*, *100*(1), 013908.

25. Kim, J. H., Yeoh, W. K., Qin, M. J., Xu, X., Dou, S. X., Munroe, P., ... & Jiang, C. H. (2006). Enhancement of in-field J c in Mg B 2/Fe wire using single-and multiwalled carbon nanotubes. *Applied Physics Letters*, *89*(12), 122510.

26. Shekhar, C., Giri, R., Malik, S. K., & Srivastava, O. N. (2007). Improved critical current density of MgB2–carbon nanotubes composite. *Journal of nanoscience and nanotechnology*, *7*(6), 1804-1809.

27. Sawada, M., Shimoyama, J. I., Takagi, N., Motoki, T., Kodama, M., & Tanaka, H. (2018). A new carbon source MgB2C2 for the synthesis of carbon-doped MgB2 materials. *Solid State Communications*, *281*, 53-56.

28. Tolendiuly, S., Fomenko, S. M., Dannangoda, G. C., & Martirosyan, K. S. (2017). Self-Propagating High Temperature Synthesis of MgB2 Superconductor in High-Pressure of Argon Condition. *Eurasian Chemico-Technological Journal*, *19*(2), 177-181.

29. *IUPAC. Compendium of Chemical Terminology, 2nd ed. (the "Gold Book"). Compiled by A. D. McNaught and A. Wilkinson. Blackwell Scientific Publications, Oxford (1997).*

30. Nishijima, G., Ye, S. J., Matsumoto, A., Togano, K., Kumakura, H., Kitaguchi, H., & Oguro, H. (2012). Mechanical properties of MgB2 superconducting wires fabricated by internal Mg diffusion process. *Superconductor Science and Technology*, *25*(5), 054012.

31. Katagiri, K., Takaya, R., Kasaba, K., Tachikawa, K., Yamada, Y., Shimura, S., ... & Watanabe, K. (2005). Stress–strain effects on powder-in-tube MgB2 tapes and wires. *Superconductor Science and Technology*, *18*(12), S351.

32. Chen, S. K., Tan, K. S., Glowacki, B. A., Yeoh, W. K., Soltanian, S., Horvat, J., & Dou, S. X. (2005). Effect of heating rates on superconducting properties of pure MgB 2, carbon nanotube-and nano-SiC-doped in situ MgB 2⁄ Fe wires. *Applied Physics Letters*, *87*(18), 182504.

33. Dou, S. X., Yeoh, W. K., Shcherbakova, O., Wexler, D., Li, Y., Ren, Z. M., ... & MacManus-Driscoll, J. L. (2006). Alignment of carbon nanotube additives for improved

performance of magnesium diboride superconductors. *Advanced Materials*, *18*(6), 785-788.

34. Tolendiuly, S., Fomenko, S. M., Abdulkarimova, R. G., Mansurov, Z. A., Dannangoda, G. C., & Martirosyan, K. S. (2016). The effect of MWCNT addition on superconducting properties of MgB 2 fabricated by high-pressure combustion synthesis. *International Journal of Self-Propagating High-Temperature Synthesis*, *25*(2), 97-101.

35. Wang, D., Ma, Y., Yu, Z., Gao, Z., Zhang, X., Watanabe, K., & Mossang, E. (2007). Strong influence of precursor powder on the critical current density of Fe-sheathed MgB2 tapes. *Superconductor Science and Technology*, *20*(6), 574.

36. Fischer, C., Rodig, C., Häßler, W., Perner, O., Eckert, J., Nenkov, K., ... & Schultz, L. (2003). Preparation of MgB 2 tapes using a nanocrystalline partially reacted precursor. *Applied physics letters*, *83*(9), 1803-1805.

37. Fang, H., Padmanabhan, S., Zhou, Y. X., & Salama, K. (2003). High critical current density in iron-clad MgB 2 tapes. *Applied physics letters*, *82*(23), 4113-4115.

38. Hobosyan, M. A., Martinez, P. M., Zakhidov, A. A., Haines, C. S., Baughman, R. H., & Martirosyan, K. S. (2017). Laminar composite structures for high power actuators. *Applied Physics Letters*, *110*(20), 203101.

39. Jauncey G. E. (1924). The Scattering of X-Rays and Bragg's Law. *Proceedings of the National Academy of Sciences of the United States of America*, *10*(2), 57–60. doi:10.1073/pnas.10.2.57.

40. K. S. Martirosyan, C. Dannangoda, E. Galstyan, and D. Litvinov, Screen-printing of ferrite magnetic nanoparticles produced by carbon combustion synthesis of oxides, J. Appl. Phys., 111, 094311, 2012.

41. K.S. Martirosyan and D. Luss, Fabrication of metal oxides nanoparticles by highly exothermic reactions, Chem. Eng. Technology, 32, 9, 1376-1383, 2009.

42. Martirosyan, K. S., & Luss, D. (2011). *U.S. Patent No. 7,897,135*. Washington, DC: U.S. Patent and Trademark Office.

43. Martirosyan, K. S., Iliev, M., & Luss, D. (2007). Carbon combustion synthesis of nanostructured perovskites. *International Journal of Self-Propagating High-Temperature Synthesis*, *16*(1), 36-45.

44. K.S. Martirosyan, E. Galstyan, Y.Y. Xue and D. Luss, The fabrication of YBCO superconductor polycrystalline powder by CCSO, *Superconductor Science and Technology*, 21, 065008, 2008.

45. Langford, J. I., & Wilson, A. J. C. (1978). Scherrer after sixty years: a survey and some new results in the determination of crystallite size. *Journal of applied crystallography*, *11*(2), 102-113.

46. Cullity, B. D., & Graham, C. D. (2011). *Introduction to magnetic materials*. John Wiley & Sons.

47. Buzea, C., & Yamashita, T. (2001). Review of the superconducting properties of MgB_2. *Superconductor Science and Technology*, *14*(11), R115.

48. Bean, C. P. (1962). Magnetization of hard superconductors. *Physical review letters*, *8*(6), 250.

BIOGRAPHICAL SKETCH

Ujjal Lamichhane was born on the 11th of March 1991 in Jantadihi, 04 Panchkhal, Kavepalanchok, Nepal. He received his Bachelor of Science in Physics from Tribhuvan University in 2012 and Master of Science in Physics from the same university in 2015 with non-thesis option. He obtained his Master of Science in Physics with thesis option from the University of Texas Rio Grande Valley on the May 2020, where he had worked as a Graduate Teaching Assistant. He is interested in Material Science and experimental Condensed Matter Physics. His personal email is brightujjal2@gmail.com.